Emerging Disinfection Byproduct 2,6-Dichlorobenzoquinone-Induced Cardiovascular Developmental Toxicity of Embryonic Zebrafish and Larvae: Imaging and Transcriptome Analysis

Xue Yang, Chang Wang,* Qi Zheng, Qiongyu Liu, Nicholas J. P. Wawryk, and Xing-Fang Li*

Cite This: ACS Omega 2022, 7, 45642−45653

Read Online

ACCESS | Metrics & More | Article Recommendations | SI Supporting Information

ABSTRACT: Epidemiological studies have observed the potential association of water disinfection byproduct (DBP) exposure with cardiac defects. Aromatic DBPs represent a significant portion of total DBPs, but their effects on cardiovascular development are unclear. In this study, we examined the effects of an aromatic DBP, 2,6-dichlorobenzoquinone (DCBQ), on the cardiovascular development of zebrafish embryos. After exposure to 2, 4, and 8 μM DCBQ, morphological images of growing zebrafish embryos clearly showed cardiovascular malformation. Fluorescent images of transgenic zebrafish strains with fluorescently labeled heart and blood vessels show that DCBQ exposure resulted in deformed atrium−ventricle looping, degenerated abdomen and trunk vessels, pericardial edema, and decreased blood flow. Furthermore, the expression of the marker gene *myl7* (essential for the differentiation and motility of cardiomyocytes) was inhibited in a dose-dependent manner by DCBQ exposure. Finally, transcriptome analysis found that in the 4 μM DCBQ exposure group, the numbers of differentially expressed genes (DEGs) were 113 (50 upregulated and 63 downregulated) at 24 hpf, 2123 (762 upregulated and 1361 downregulated) at 48 hpf, and 61 (11 upregulated and 50 downregulated) at 120 hpf; in the 8 μM DCBQ exposure group, the number of DEGs was 1407 (647 upregulated and 760 downregulated) at 120 hpf. The FoxO signaling pathway was significantly altered. The *in vivo* results demonstrate the effects of 2,6-DCBQ (0−8 μM) on cardiovascular development, contributing to the understanding of the developmental toxicity of aromatic DBP halobenzoquinones (HBQs).
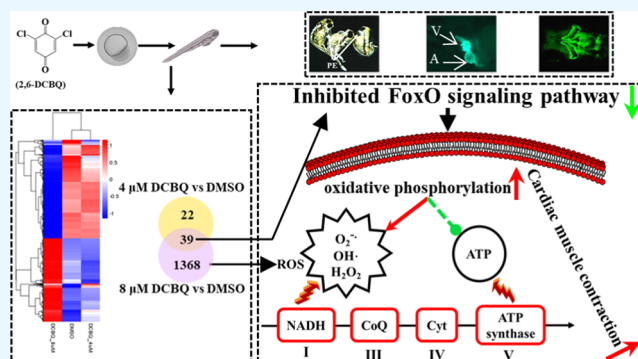
1. INTRODUCTION

Drinking water disinfection effectively inactivates pathogenic microorganisms in water and significantly reduces the incidence of waterborne disease. However, disinfectants can react with natural organic substances or environmental pollutants in source water to produce a variety of disinfection byproducts (DBPs).[1−6] Some epidemiological studies have shown the association between DBPs and adverse developmental outcomes.[7−9] A recent meta-analysis has shown an increased risk of small for gestational age (SGA) birth defect associated with exposure to the regulated DBPs trihalomethanes (THMs).[10] In addition, previous studies have shown that exposure to DBPs during pregnancy may increase maternal oxidative stress,[11] which is proposed to play a critical role in the pathogenesis of adverse fetal development.[12,13] There is a lack of information on the effects of emerging aromatic DBPs on the development of the cardiovascular system.

Aromatic halogenated DBPs occur widely in drinking water and represent a significant portion of total halogenated DBPs.[3,4,14−16] Recent studies have found that aromatic DBPs can reach concentrations as high as 120 μg/L as Cl based on

the well-designed measurements of total organic halogens (TOX) in chlorinated water samples.[16,17] Aromatic DBPs are generally more cytotoxic than aliphatic ones[16,18] and some *in vivo* bioassays have also demonstrated higher developmental toxicity and growth inhibition induced by aromatic DBPs compared with aliphatic ones.[19−21] Halogenated benzoquinones (HBQs) are a group of aromatic DBPs that have been widely detected in halogen-disinfected drinking water and swimming pools.[15,22,23] HBQs are significantly more cytotoxic than the regulated DBPs. The toxicity of HBQs has been tested using *in vitro* models such as the Chinese hamster ovary (CHO-K1)[24] and human cell lines (T24, HepG2, hNSCs, and SV-HUC-1).[25−28] HBQs can induce the generation of reactive oxygen species (ROS) and the reduction of glutathione (GSH), resulting in damage to DNA and functional proteins.[25]
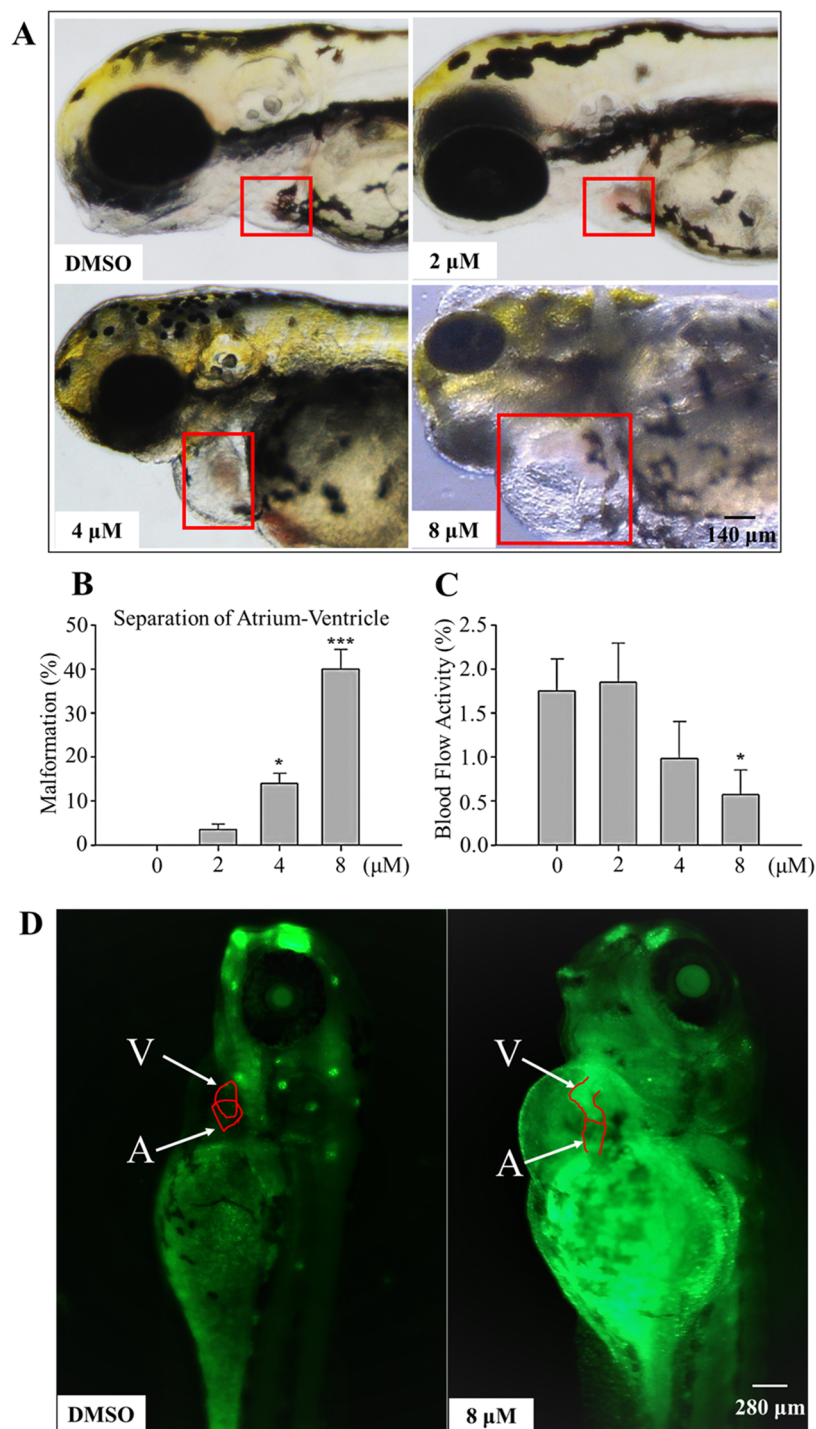
Figure 1. Effects of DCBQ exposure on the zebrafish larvae (A) morphology; (B) percentage of atrial−ventricular separation; (C) blood flow activity after exposure to DCBQ (0, 2, 4, and 8 μM) for 72 hpf; (D) visualization of apoptotic cells using AO staining at 96 hpf in zebrafish larvae in the control group (dimethyl sulfoxide, DMSO) and the treatment group (8 μM 2,6-DCBQ). V represents the ventricle; A represents the atrium. Error bars indicate the mean $\pm$ standard error of the mean (SEM). Triple replicate experiments were performed for each exposure group (n = 3). Analysis of variance (ANOVA) with Dunnett's post-test: *$p < 0.05$, **$p < 0.01$, ***$p < 0.001$.

The effects of 2,6-dichlorobenzoquinone (2,6-DCBQ) on gene expression revealed its significant alteration of oxidative stress signaling pathways in human uroepithelial cells.[27] Exposure to HBQs can cause oxidative stress resulting in deformation in zebrafish embryos.[29] However, the toxicological effect of aromatic DBPs on the cardiovascular system remains unclear.

Zebrafish are widely used for studying the developmental effects and molecular mechanisms of environmental contam-inants.[30] The embryogenesis is rapid: the fertilized eggs develop into embryos in 24 h. At 36 hpf, most organ primordia are established, including the nervous system and contractile heart tube, as well as blood circulation.[31] The cardiovascular system is one of the first embryonic organs developed with morphological plasticity. Blood vessels are an integral part of the organism, vital to organ function, and essential for embryonic development.[32,33] Several recently developed trans-
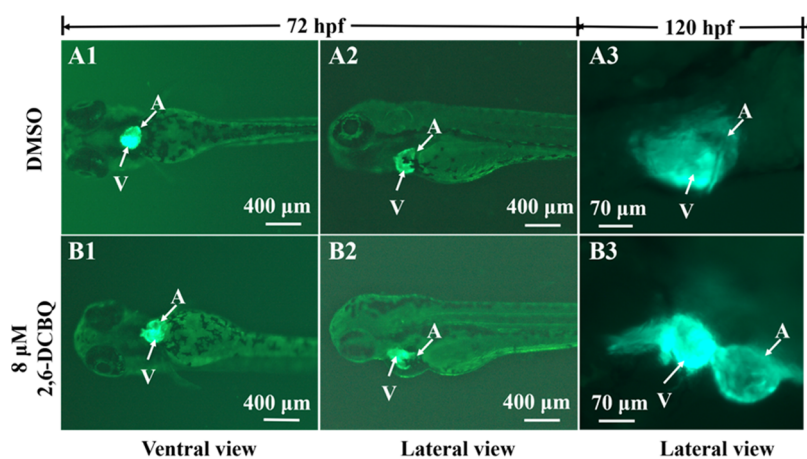
Figure 2. Representative images of the contour of atrium–ventricle with green fluorescence from ventral and lateral views in the control group (A) and the 8 μM 2,6-DCBQ treatment group (B) at 72 hpf and 120 hpf. V represents the ventricle; A represents the atrium.

genic zebrafish lines can express fluorescent reporter proteins in cardiovascular tissues and enable the imaging and molecular studies of cardiovascular development in live embryos during chemical exposure.[34] Therefore, we used the wild-type and two transgenic strains of embryonic zebrafish to investigate the effects of aromatic DBPs on cardiovascular development.

In this study, we examined the effects of 2,6-DCBQ on the cardio-development of two strains of transgenic zebrafish (T_g (zp3:fsta, myl7:EGFP) and T_g (kdrl:EGFP)). The T_g (zp3:fsta, myl7:EGFP) transgenic zebrafish is cloned with the EGFP cassette along the downstream of zp3:fst1-polyA, and the promotor elements of *myl*7 control the EGFP expression in heart tissue. The T_g (kdrl:EGFP) transgenic zebrafish is cloned with the EGFP cassette along the downstream of the *kdrl* promoter, which specifically regulates the EGFP expression in vascular tissue. The two strains enabled us to clearly observe heart and blood vessel development after exposure to varying concentrations of DCBQ. First, we examined the development of the heart and blood vessels by analyzing the rate of abnormal cardiovascular development events and blood flow activity. Second, we investigated the spatial expression changes of the heart-specific expression gene *myl*7 using whole-mount *in situ* hybridization (WISH) and determined the relative expression level of the *myl*7 gene using quantitative real-time polymerase chain reaction (qRT-PCR). Finally, we investigated transcriptome changes to explore the potential mechanism of cardiovascular toxicity.

2. RESULTS AND DISCUSSION

2.1. Acute and Developmental Toxicity of 2,6-DCBQ on Zebrafish Embryos. The dose–response curves were obtained for the three types of zebrafish (wild AB, T_g (zp3:fsta, myl7:EGFP), and T_g (kdrl:EGFP)) after exposure to DCBQ (0, 1, 2, 4, 5, 8, 10, and 16 μM) at 24 and 48 hpf (Figure S1). The average lethal concentration 50 (LC_{50}) was 5.9 ± 0.3 μM for all three strains after exposure to 2,6-DCBQ (0, 1, 2, 4, 5, 8, 10, 16 μM). Figure 1 presents the concentration-dependent effects of DCBQ on the development of the embryos' (A) morphology, (B) separation of atrium–ventricle, and (C) blood flow activity after exposure to DCBQ (0, 2, 4, and 8 μM) for 72 hpf. DCBQ induced significant separation between pericardial edema and atrium–ventricle which was clearly observed in the 4 and 8 μM groups (Figure 1A), while the separation in the 2 μM group was not visible. As shown in

Figure 1B, the malformation rate of atrium–ventricle separation was significantly increased by 13.3% in the 4 μM and 40.0% in the 8 μM groups. As shown in Figure 1C, a decrease in the blood flow activity was observed in both the 4 and 8 μM groups but not in the 2 μM group; the decrease of the blood flow activity in the 8 μM groups was statistically significant. As previously reported, the deformation in a heart structure can decrease the heart rate and blood flow activity as the distance of atrium–ventricle indicates progressive heart looping.[29,35,36] Additionally, we observed a significant increase in the number of apoptotic cells in the AO-stained larvae (8 μM groups) compared with the controls, as shown in Figure 1D. These results suggest that 2,6-DCBQ exposure can result in abnormalities in cardiovascular development, including atrium–ventricle separation, pericardial edema, and decrease in the heart rate and blood flow activity, and induce cell apoptosis in the heart and the abdomen.

2.2. Fluorescence Imaging of Cardiovascular Toxicity of DCBQ in Transgenic Larvae. To visualize the effects of 2,6-DCBQ exposure on the atrium–ventricle of zebrafish, we used two transgenic zebrafish strains T_g (zp3:fsta, myl7:EGFP)[37] and T_g (kdrl:EGFP).[38] Exposure experiments were performed with varying concentrations of 2,6-DCBQ. Clear images showing the deformation of the cardiovascular system were obtained from the 8 μM groups. As shown in Figure 2, the contour of atrium (A)–ventricle (V) was visualized with green fluorescence from the ventral and lateral views. In the control group, the normal looping process placed the ventricle and atrium side by side, so the two chambers largely overlapped with each other in the lateral view. In contrast, enlarged heart and pericardial edema were observed after exposure to 8 μM 2,6-DCBQ for 72 hpf. With exposure time increasing to 120 hpf, shorter atrial–ventricular looping and linearized heart tube were clearly observed in the treated zebrafish. These results demonstrate severe defects during the heart looping process, which is highly associated with abnormal heart rate and blood circulation.[39–42]

The vascular tissue of T_g (kdrl:EGFP) larvae specifically expressed EGFP. The developing zebrafish have six aortic arches (AAs) in the ventral head of embryonic zebrafish: the mandibular arch (AA1), the opercular artery (ORA), the third aortic arches (AA3), the fourth aortic arches (AA4), the fifth aortic arches (AA5), and the sixth aortic arches (AA6) at 120 hpf.[43] Figure 3 shows the effects of 2,6-DCBQ exposure on
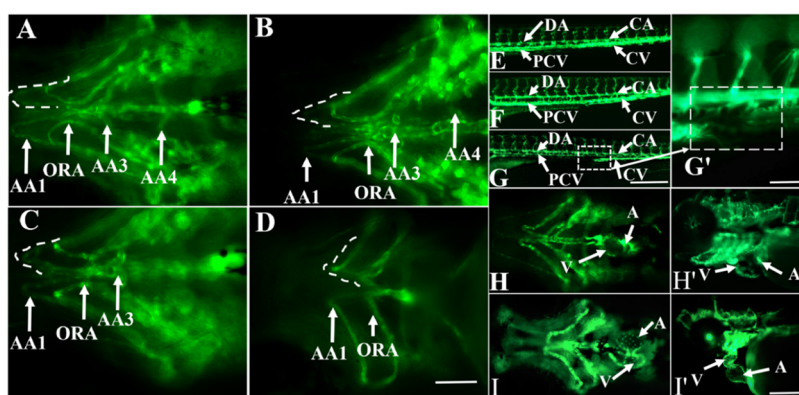
Figure 3. Development of the aortic arches (A–D) and blood vessels (E–G) in transgenic zebrafish larvae T_g (kdrl:EGFP) after exposure to DMSO and 2, 4, and 8 μM 2,6-DCBQ at 120 hpf. Magnification (G′) for the rupture of the posterior main vein and tail vein in (G). The development of the heart from the ventral view (H, I) and from the lateral view (H′, I′) in transgenic zebrafish larvae T_g (kdrl:EGFP) after exposure to DMSO and 4 μM 2,6-DCBQ at 120 hpf. (A–D) scale bar is 100 μm, (E–G) scale bar is 400 μm, (G′) scale bar is 50 μm, and (H–I′) scale bar is 200 μm. AA1: mandibular arch; ORA: opercular artery; AA3: third aortic arches, AA4: fourth aortic arches; DA: dorsal aorta; PCV: posterior cardinal vein; CA: caudal artery; CV: caudal vein; V: ventricle; A: atrium.
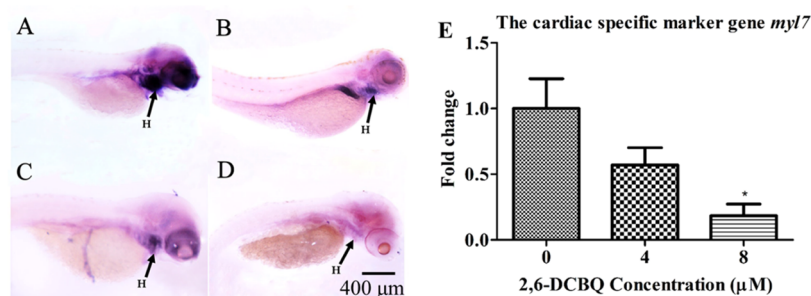
Figure 4. (A–D) *In situ* expression of the *myl7* gene in zebrafish larvae after exposure to DMSO (control) and 2, 4, and 8 μM 2,6-DCBQ at 96 hpf. (E) Expression profiles of *myl7* in zebrafish larvae after exposure to 2,6-DCBQ (0, 2, 8 μM) at 120 hpf. Error bars indicate the mean ± SEM. Four replicate experiments were performed for each exposure group. (A–D) Scale bar 400 μm. H represents the heart.

vascular and cardiac dysplasia in T_g (kdrl:EGFP) larvae. The vascular endothelial cells in the AAs of T_g (kdrl:EGFP) zebrafish larvae were significantly reduced in the 2 and 4 μM 2,6-DCBQ treatment groups at 120 hpf (Figure 3B,C). The lack of AA4 was detected in the 4 and 8 μM exposure groups (Figure 3C,D), while the lack of AA3 was also observed in the 8 μM group. Furthermore, 2,6-DCBQ promoted abnormal angiogenesis in the dorsal aorta (DA), posterior cardinal vein (PCV), caudal artery (CA), caudal vein (CV), and the surrounding blood vessels compared to the control group (Figure 3E–G). A rupture was particularly observed in the connection between the posterior main vein and the tail vein in the exposure group of 8 μM 2,6-DCBQ (Figure 3G,G′). Previous studies have shown that abnormal development of blood vessels may be related to the lack of hemodynamics and shear force.[44] Moreover, in the ventral and lateral views of the heart, 2,6-DCBQ exposure led to less looping of atrium–ventricle (Figure 3H,I,H′,I′). In short, the visualization analysis clearly showed 2,6-DCBQ-induced dysplasia in the cardiovascular system.

2.3. Whole-Mount *In Situ* Hybridization for Cardiac Progenitor Cell Marker Gene *myl7*. The *myl7* gene is dominantly expressed in the cardiac muscle atria and is necessary for the differentiation, motility function, and myocardial contractility of zebrafish heart cardiomyocytes.[45] Therefore, we examined the *in situ* expression of *myl7* following 2,6-DCBQ exposure using WISH. Figure 4A–D

clearly shows that 2,6-DCBQ inhibited the *myl7* expression in the heart area in a dose-dependent manner. Furthermore, qRT-RCR analysis also confirmed the downregulation of *myl7* expression (Figure 4E). Our results of the deformed atria, ventricle looping, and pericardial edema, as well as the functional impact on decreasing heart rate and blood flow activity, clearly support that the cardiovascular system damage was induced by DCBQ. This is consistent with previous studies showing that the downregulation of *myl7* resulted in failure of the development of cardiomyocytes, cardiac developmental defects,[46] and decreased contractility of embryonic atrium–ventricle.[47]

2.4. Transcriptome Analysis of Cardiovascular Toxicity. *2.4.1. Global Gene Changes and Principal Component Analysis.* To explore the molecular mechanism of cardiovascular dysplasia induced by 2,6-DCBQ, we carried out transcriptome analysis using Illumina deep sequencing. The sequencing data for all samples met quality assurance (QA) requirements, and the results are shown in the Supporting Information (Table S2). At 24 and 48 hpf, the number of differentially expressed genes (DEGs) in the 4 μM treatment group was 113 (50 upregulated and 63 downregulated) and 2123 (762 upregulated and 1361 downregulated), respectively, compared to the control group (Figure S2). At 120 hpf, 61 (11 upregulated and 50 downregulated) and 1407 (647 upregulated and 760 downregulated) DEGs were identified in the 4 and 8 μM 2,6-DCBQ treatment groups (Figure 5A,B),
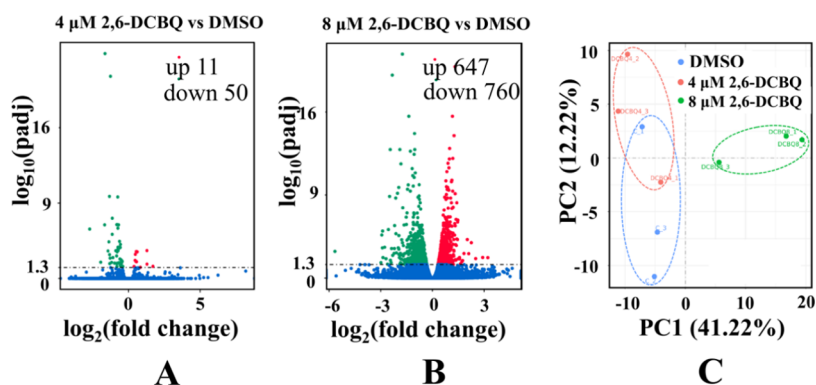
Figure 5. (A, B) Volcano map of the differential gene in transcriptome analysis after exposure to 2,6-DCBQ (4, 8 μM) relative to the control group at 120 hpf. (C) PCA plot, the percentage values represented the contribution of the first (PC1) and second (PC2) principal components. Each treatment (three replicates) is depicted in a different color.
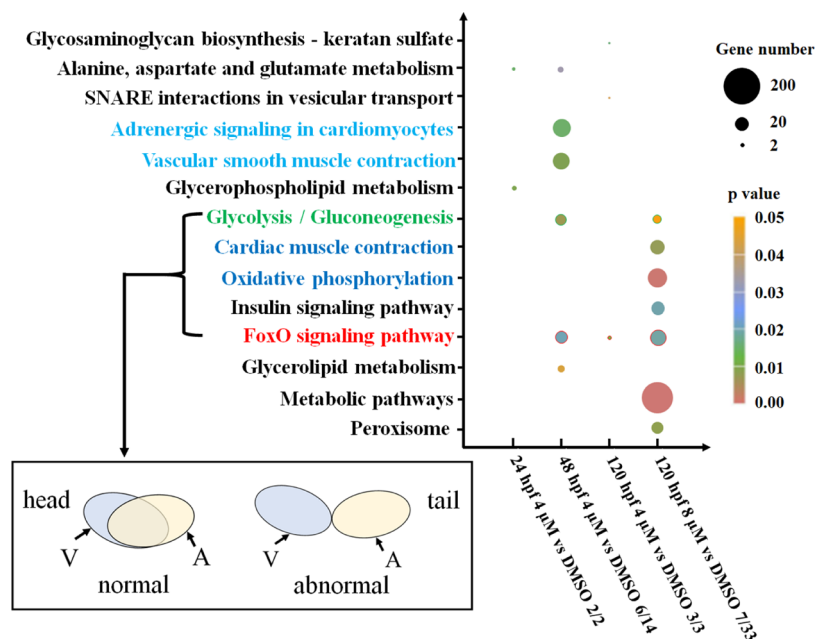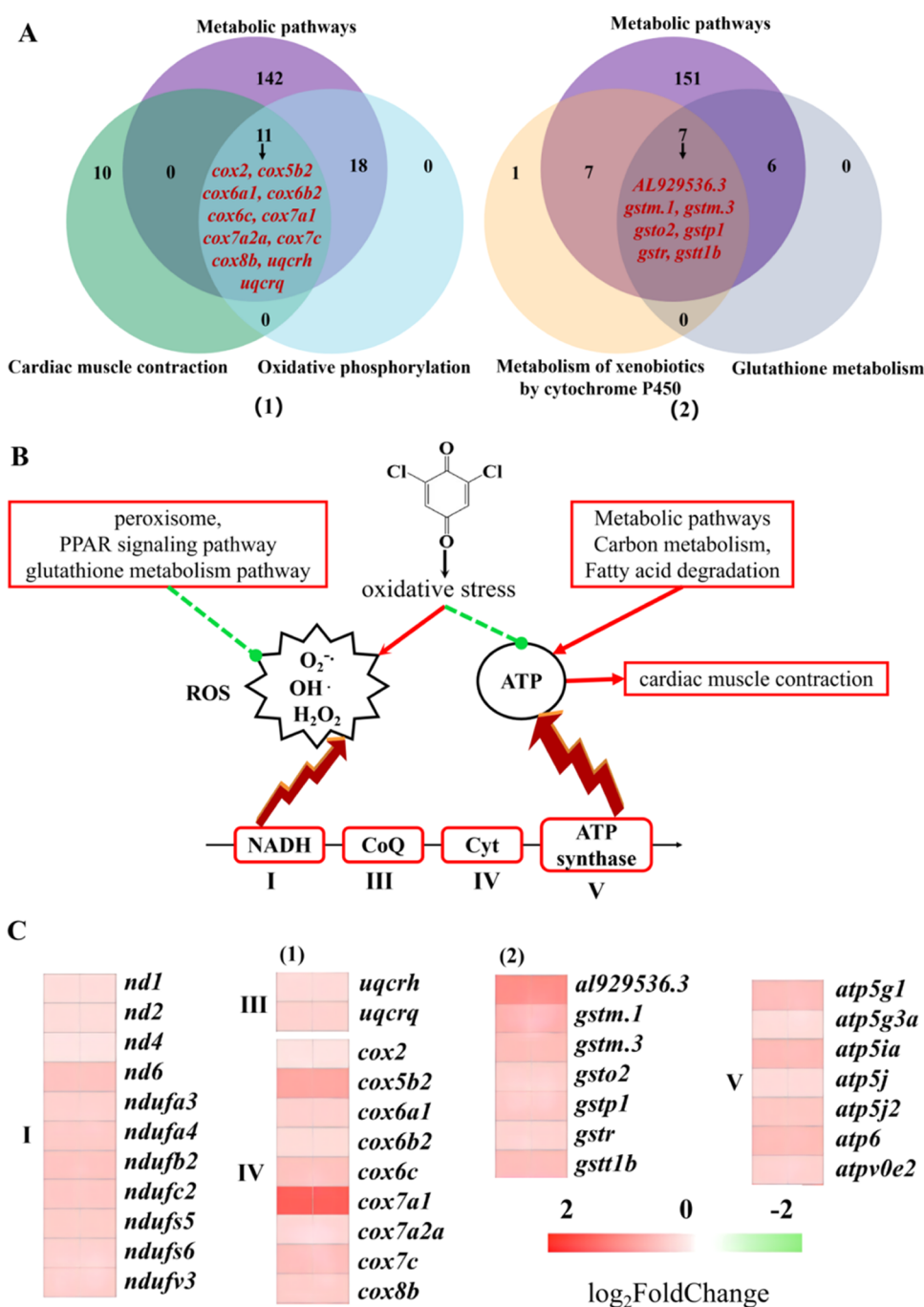

Figure 6. Comparison of the KEGG pathway between different exposure groups based on cardiovascular development. The bottom left image indicates the schematic representation of normally and abnormally developing cardiac structures, containing the ventricle (V) and the atrium (A) with the head on the left and the tail on the right for zebrafish.

respectively, compared to the control group. The two-dimensional (2D) PCA (Figure 5C) plot was produced based on the log fragments per kilobase per million (FPKM) values of each sample. The PCA demonstrated that the DMSO group was partially overlapped with the 4 μM 2,6-DCBQ treatment group, but highly separated from the 8 μM 2,6-DCBQ treatment group at the transcriptional levels. For the 4 μM exposure group, a larger number of DEGs were induced by 48 h exposure than by 120 h exposure. The results suggested that 4 μM 2,6-DCBQ significantly affected the development of embryos in the early stage of exposure, and the expression of most genes recovered to the original level. On the contrary, the number of DEGs in the 8 μM exposure group at 120 hpf was significantly increased compared to the 4 μM exposure group at 120 hpf, which indicated that 8 μM exposure induced irreversible damage. This also explains the higher malformation rate in the 8 μM exposure group.

2.4.2. Perturbation of the FoxO Signaling Pathway. In the 4 μM 2,6-DCBQ treatment group, 2 and 14 KEGG pathways

were significantly enriched at 24 and 48 hpf, respectively (Table S3). At 120 hpf, 3 and 33 KEGG pathways were significantly enriched in the 4 and 8 μM 2,6-DCBQ treatment groups, respectively (Table S4). Given these results, we compared the signaling pathways related to cardiovascular development that were significantly enriched at these three exposure time points (24, 48, and 120 hpf) in the 4 μM exposure group, as well as in the 8 μM exposure group at 120 hpf (Figure 6). The FoxO signaling pathway was significantly enriched in both the 4 μM (48 and 120 hpf) and the 8 μM (120 hpf) 2,6-DCBQ exposure groups. In the FoxO signaling pathway, 14 DEGs (4 upregulated and 10 downregulated) were enriched in the 4 μM 2,6-DCBQ exposure groups at 48 hpf (Table S5), while 2 DEGs (one upregulated and one downregulated) and 22 DEGs (6 upregulated and 16 downregulated) were enriched in the 4 and 8 μM 2,6-DCBQ treatment groups at 120 hpf (Table 1), respectively. This result suggested that the FoxO signaling pathway may be a potential target signaling pathway for DCBQ exposure. Furthermore, it

Table 1. DEGs Enriched in the FoxO Signaling Pathway[a]

gene	description	regulation	Log$_2$FoldChange
sgk1	serum/glucocorticoid-regulated kinase 1	down	−0.43468
gadd45aa	growth arrest and DNA-damage-inducible protein	up	0.55435
cr354588.1	insulin receptor substrate 2-b-like	down	−0.58402
egfra	epidermal growth factor receptor a	down	−0.42387
foxo1a	forkhead box o1 a	down	−0.49338
foxo1b	forkhead box o1 b	down	−1.8518
foxo3b	forkhead box o3b	down	−0.44497
foxo4	forkhead box o4	down	−0.33137
gadd45bb	growth arrest and DNA-damage-inducible, β b	down	−0.51512
igf1ra	insulin-like growth factor 1a receptor	down	−0.83213
ikbkb	inhibitor of kappa light polypeptide gene enhancer in b-cells, kinase β	down	−0.61939
insrb	insulin receptor b	down	−0.63288
irs2a	insulin receptor substrate 2a	down	−0.52649
irs2b	insulin receptor substrate 2b	down	−0.70728
klf2b	Kruppel-like factor 2b	down	−0.44855
pik3ca	phosphatidylinositol-4,5-bisphosphate 3-kinase, catalytic subunit α	down	−1.0023
sgk1	serum/glucocorticoid-regulated kinase 1	down	−0.6783
stat3	signal transducer and activator of transcription 3 (acute-phase response factor)	down	−0.85427
cat	catalase	up	0.48953
ccnb1	cyclin b1	up	0.86071
pck2	phosphoenolpyruvate carboxykinase 2 (mitochondrial)	up	0.39871
plk1	polo-like kinase 1 (drosophila)	up	0.57741
sod2	superoxide dismutase 2, mitochondrial	up	0.4126
tnfsf10	tumor necrosis factor (ligand) superfamily, member 10	up	0.64513

[a]Gray background indicates DEGs in the 4 μM 2,6-DCBQ exposure group; white background indicates DEGs in the 8 μM 2,6-DCBQ exposure group.

Figure 7. Schematic map of the enriched FoxO signaling pathway. Red color box: significant increase; green color box: significant decrease.

is interesting that the signaling pathway of glycolysis/gluconeogenesis was both significantly enriched in the 4 μM exposure group at 48 hpf and in the 8 μM exposure group at 120 hpf, suggesting that DCBQ exposure affects energy metabolism. However, the two signaling pathways, cardiac muscle contraction, and oxidative phosphorylation were only

Figure 8. (A) Venn diagrams of five significantly enriched signaling pathways for DEGs, of which (1) indicates that 11 DEGs are enriched in three signaling pathways (cardiac muscle contraction, metabolic pathways, and oxidative phosphorylation), and (2) indicates that 7 DEGs are enriched in three signaling pathways (metabolic pathways, metabolism of xenobiotics by cytochrome P450, and glutathione metabolism). (B) The schematic mechanism for 2,6-DCBQ exposure: the red solid line arrow indicates an increase or activation, the green dotted line arrow with the round end indicates a decrease or depletion, and the red border indicates activation. (C) The heat map of the detailed expression of genes of the glutathione S-transferase family and of the subunits that are assembled as the complex (I, III, IV, V) in the 8 μM 2,6-DCBQ treatment group, expressed as the log$_2$FoldChange compared to the control.

significantly enriched in the 8 μM exposure group at 120 hpf. This finding may explain the potential mechanisms of the effects of DCBQ on morphological and cardiovascular abnormalities and mortality in embryos at acute toxicity. The following discussion focuses on the transcriptome analysis in the 8 μM exposure group at 120 hpf.

Figure 7 shows the details of the FoxO signaling pathway regulated by these DEGs in the 8 μM 2,6-DCBQ exposure

groups. Recent studies reported that FoxO pathways have been identified as therapeutic targets for several major heart diseases, such as ischemic heart disease and diabetic cardiomyopathy.[48] Additionally, FoxO activity is mainly regulated by the insulin signaling pathway and PI3K-Akt signaling.[49,50] Meanwhile, some evidence has suggested that three members of the FoxO subfamily, FoxO1, FoxO3, and FoxO4, are essential in maintaining cardiac function and

mediating cardiac stresses, which are inhibited by growth factors, such as insulin and insulin-like growth factor-1.[51] The FoxO family is considered to be involved in the regulation of cardiac function by controlling oxidative stress resistance,[52] glycolysis/gluconeogenesis, cell cycle, and apoptosis[53] in the cardiovascular system. In this study, our results showed that the upstream of the FoxO signaling pathway, the insulin signaling pathway, was distinctly inhibited after 8 μM 2,6-DCBQ exposure, including 16 down- and 4 upregulated genes (Table S6). Inhibition of the insulin signaling pathway can promote cardiovascular damage, reprogram stem cardiac cells, and increase the risk of heart disease in diabetic patients.[54] In addition, the aggravation of myocardial injury and myocardial infarction was induced by the inhibition of the insulin signaling pathway.[55] Eight key genes (insrb, irs2a, irs2b, pik3ca, ikbkb, foxo1a, foxo1b, and pck2) in the insulin and FoxO pathways were regulated. In the upstream, insulin receptor-related factors insrb, irs2a, and irs2b were significantly downregulated by 1.55-fold, 1.44-fold, and 1.63-fold, respectively, after DCBQ exposure. Evidence suggested that the depletion of insulin receptors can lead to pericardial edema and abnormal cardiac morphology.[56,57] Foxo1a and foxo1b were significantly downregulated by 1.40-fold and 3.61-fold, respectively, after DCBQ exposure. The foxo1 gene is a critical regulator of vascular growth in addition to regulating the metabolic and proliferative activities in endothelial cells.[58] These results support that cardiovascular toxicity induced by 2,6-DCBQ is at least partially due to the inhibition of insulin and FoxO signaling pathways. Therefore, further analysis of the altered genes in FoxO and insulin signaling pathways is necessary to better understand the effect of 2,6-DCBQ on cardiovascular development.

2.4.3. DCBQ Elicited Responses of Respiratory Electron Transport Chain and Oxidative Damage.

The top ten term KEGG signaling pathways of the 8 μM 2,6-DCBQ treatment group are catabolism pathways, including oxidative phosphorylation, PPAR signaling pathway, xenobiotics metabolism (cytochrome P450), drug metabolism, amino acid metabolism (glycine, serine, and threonine), carbon metabolism, fatty acid degradation, cardiac muscle contraction, and glutathione metabolism. In the cardiac muscle contraction pathway, nearly 13.5% DEGs were significantly changed (17 upregulated and 4 downregulated) (Table S7), and the regulation of DEGs in this signaling pathway is shown in the Supporting Information (Figure S3). Furthermore, we found that 11 upregulated genes (cox2, cox5b2, cox6a1, cox6b2, cox6c, cox7a, cox7a2a, cox7c, cox8b, uqcrq, and uqcrh) enriched in these three signaling pathways (cardiac muscle contraction, metabolic pathways, and oxidative phosphorylation pathway) (Figure 8A,C), are the cyclooxygenase (COX) subunits. A recent study reported that exposure to nitro-PAHs may increase oxidative stress, change the activity of the COX family, and adversely affect cardiovascular health.[59] We found that DCBQ upregulated 7 genes (al929536.3, gstm.1, gstm.3, gsto2, gstp1, gstr, and gstt1b) enriched in three signaling pathways: metabolic pathways, xenobiotics metabolism (cytochrome P450), and glutathione metabolism. These belong to the glutathione S-transferase family. It has been shown that glutathione S-transferases play an important role in phase II of detoxification to protect cells in response to oxidative stress generated by exogenous toxicants.[60,61] These findings indicate that exposure to 2,6-DCBQ induced severe oxidative stress and activated a multistage antioxidant defense system.

Notably, in the oxidative phosphorylation pathway, 29 DEGs were upregulated. Coincidently, these genes are the subunits that are assembled as the complex (I, III, IV, V) (Figure 8B) of the respiratory electron transport chain. These complexes constitute the NADH oxidation respiratory chain located in the mitochondrial inner membrane. Mitochondria produce most of the adenosine triphosphate (ATP) required for cardiac contractile activity.[62] In the respiratory electron transport chain, superoxide anions are quickly converted to the less reactive H_2O_2 by superoxide dismutase. In addition to being a byproduct, hydrogen peroxide participates in various signaling pathways and pivotal cellular processes.[63] Halogenated benzoquinones can catalyze the formation of hydroxyl radicals from hydrogen peroxide by a transition-metal ion-independent Fenton reaction.[64] Additionally, 2,5-dichlorobenzoquinone can promote the decomposition of hydroperoxide by the formation of an unusual carbon-centered quinone ketoxy radical without the action of metal ions.[65] Therefore, DCBQ may disrupt redox homeostasis, generate highly reactive free radicals from hydrogen peroxide, and finally induce oxidative damage in multiple tissues and cell lines.[27,29] However, a positive correlation between severe oxidative stress and ATP depletion has been determined.[66,67] Hence, our results showed that oxidative phosphorylation was abnormally activated to produce more ATP for cardiac muscle contraction, and catabolism pathways were activated to increase ATP. Meanwhile, the anti-oxidation systems including peroxisomes, the PPAR signaling pathway, and glutathione metabolism pathway were activated to protect the organism against damage from ROS ($O_2^{-\bullet}$, $OH^\bullet$, and H_2O_2) produced via the electron transport chain or DCBQ catalysis. It has been shown that peroxisomes can also protect cells from oxidative stress.[68−71] To summarize, 2,6-DCBQ exposure induced apoptosis of cardiomyocytes, pericardial edema, deformation of heart looping, and cardiac hypoplasia, and eventually led to the inhibition of flow activity and cardiac dysfunction. The heart powers the circulation of blood, which maintains the metabolism and homeostasis of various functional tissues. Heart failure may lead to the reduction of nutrient and oxygen delivery and ATP synthesis,[72] and hypoxia can elevate oxidative phosphorylation and metabolism of carbon sources to generate ATP. In addition, to resist the effects of oxidative stress, the organism abnormally activates the antioxidant system to maintain the redox balance. The schematic mechanism is shown in Figure 8B. Finally, we performed protein−protein interaction (PPI) analysis for the DEGs in the related signaling pathways: cardiac muscle contraction, oxidative phosphorylation, insulin signaling pathway, FoxO signaling pathway, and vascular endothelial growth factor (VEGF) signaling pathway (Figure S4). The PPI analysis results showed significant correlation between cardiac muscle contraction and oxidative phosphorylation. They are the upstream pathway of the FoxO signaling cascade.

3. CONCLUSIONS

This study clearly demonstrated that 2,6-DCBQ exposure significantly impacts cardiovascular development in embryonic zebrafish. Transcriptome analysis revealed that 2,6-DCBQ exposure affected the FoxO signaling pathway, myocardial contraction, and other pathways related to energy metabolism. These findings provide the basis for future investigation of molecular targets of cardiovascular toxicity, and are critical for

understanding the underlying mechanism of developmental toxicity of 2,6-DCBQ and related HBQs.

4. METHODS

4.1. Chemicals and Reagents. A 2,6-dichloro-1,4-benzoquinone (2,6-DCBQ) standard was obtained from Tokyo Chemical Industry (TCI; Toshima, Kita-ku, Tokyo, Japan) and was dissolved in dimethyl sulfoxide (DMSO), which was used as the vehicle control in each assay. Protease from *Streptomyces griseus* was used to remove chorions from embryos in earlier stages. *N*-Phenylthiourea (PTU), Sequencing Reaction Clean-Up kit (Sigma Spin), 4% paraformaldehyde (PFA), and methylcellulose were purchased from Sigma-Aldrich (St. Louis, MO).

4.2. Zebrafish Maintenance and Chemical Exposure. The wild-type AB strain, T_g (kdrl:EGFP) and T_g (zp3:fsta, myl7:EGFP) zebrafish (three months old, obtained from the Institute of Hydrobiology, Chinese Academy of Sciences) were maintained at 28 ± 0.5 °C in a 14:10 h light−dark cycle in a recirculating flow-through system in aerated water with 0.25−0.75% (w/v) salinity. The collection of zebrafish embryos was performed as described previously. Briefly, two male and two female adult fish in each tank were separated the night before the collection of fertilized eggs. In a previous study of acute toxicity of aromatic DBPs on zebrafish embryos, the doses of DBPs ranged from 0.1 to 1000 μM.[73] Exposure of zebrafish embryos to16 μM 2,6-DCBQ caused a high mortality rate (80%).[29] Hence, we examined the effects using the lower concentrations of 2, 4, and 8 μM 2,6-DCBQ. Thirty live embryos were randomly selected, placed in 6-well plates, and exposed to 2,6-DCBQ (0, 2, 4, or 8 μM) from 4 h post-fertilization (hpf) to 120 hpf. The transgenic zebrafish was selected using a fluorescence microscope at 24 hpf for subsequent phenotypic analysis, when the green fluorescent protein is expressed. The exposure time was selected based on the different developmental stages of embryonic zebrafish. At 4 hpf, healthy embryos were selected for the exposure experiments. At 72 hpf, larvae hatched and broke the chorion and morphological observation of larvae was performed. At 96 hpf, basic organogenesis and tissue differentiation was complete and *in situ* hybridization was reliably determined. All experiments were performed with three replicate wells. Both control and exposure groups contained less than 0.007% (v/v) DMSO. The study protocol was approved by the Ethics Committee of Jianghan University and performed in accordance with the guidelines for the Care and Use of Laboratory Animals of Jianghan University. All animal experiments were performed according to the Laboratory Animal Use Permit (Permit number SYXK2012-0042) issued by the Science and Technology Department of Hubei Province.

4.3. Cardiovascular System Function Assessment. The cardiac function was evaluated by counting the malformation rate of atrial and ventricular separation in zebrafish larvae after treatment with 2,6-DCBQ (0, 4, 8 μM) until 72 hpf. Blood flow activity (72 hpf) of embryos after exposure to 2,6-DCBQ (0, 2, 4, 8 μM) was measured using a DanioScope (Noldus, BV Wageningen, Netherlands) for the evaluation of the cardiovascular system function at 72 hpf. For the blood flow activity measurement, a video of blood vessels was recorded, and the blood cells present in a 1-min time window were counted in a low-speed video. The blood flow

activity was calculated by the number of blood cells per minute in the same view area.

4.4. Acridine Orange (AO) Staining. For apoptosis and whole *in situ* hybridization experiments, 96 hpf was chosen as the exposure endpoint because the development of melanin and swim bladder may influence the analysis (the smooth and reflective surface of the swim bladder could cause false positive in apoptosis experiments). After 96 hpf, the 2,6-DCBQ-treated zebrafish larvae were stained with acridine orange (AO) via the protocol referred to in the study by Wang et al. The *in situ* apoptosis of larvae cells was observed under an inverted microscope (ZEISS SteREO Discovery.V12, Germany).

4.5. Morphological Observation for Transgenic Zebrafish Lines. Two transgenic zebrafish lines T_g (kdrl:EGFP) and T_g (zp3:fsta, my17:EGFP) were used to examine the effects of 2,6-DCBQ on cardiac and vascular development, respectively. At 72 and 120 hpf, zebrafish larvae were transferred to 3% methylcellulose, then carefully observed for the assessment of cardiovascular system development via morphological analysis including the degree of atrium−ventricle looping and the size of the heart, mandibular vessels, and cardiac vessels. In addition, the cardiac contour was observed from both ventral and lateral views. The larvae were observed using a stereoscopic fluorescence microscope (ZEISS SteREO Discovery. V12, Germany).

4.6. Whole-Mount *In Situ* Hybridization. Probe primers of the *myl7* gene were designed using the Premier 5 software using the target gene sequence derived from NCBI; the primer sequences are described in the Supporting Information (Table S1). The total RNA of the larvae was extracted for reverse transcription into cDNA, and antisense RNA probes were synthesized by *in vitro* transcription using digoxigenin-labeled UTP. Details of the experimental procedures are provided in the Supporting Information.

4.7. Extraction of Total RNA for qRT-PCR and Transcriptome Analysis. After exposure to 2,6-DCBQ (0, 2, 4, 8 μM), 30 living larvae were collected for the extraction of total RNA with Trizol (Invitrogen, Burlington, ON, Canada) and genomic DNA was removed with RNase-free DNase I (Qiagen, Hilden, Germany). RNA degradation and contamination were assessed using RNase-free agarose gel electrophoresis. The quality of RNA (OD$_{260/280}$ ratio) was determined spectrophotometrically using a NanoDrop 2000c (Thermo Scientific, Rockford, IL). The expression of the *myl7* gene was measured by qRT-PCR. The housekeeping gene β-Actin was measured for quality control (QC). The details of the sample preparation and analysis are described in the Supporting Information. The GenBank accession numbers and forward and reverse primer sequences are listed in Table S1, while the fold changes in expression level were calculated using the $2^{-\Delta\Delta Ct}$ method.

The extracted total RNA was sent to Novogene Company to the company's instructions. In brief, the total RNA of the seven exposure groups (24 hpf for 4 μM vs DMSO; 48 hpf for 4 μM vs DMSO; 120 hpf for 8 μM vs DMSO, and 4 μM vs DMSO) were used to construct the cDNA libraries by reverse transcription. These libraries were assessed for quality on an Agilent Bioanalyzer 2100 system, normalized, and pooled for sequencing. Raw sequencing reads were de-multiplexed from image data on the Illumina HiSeq 2500 platform by Illumina's CASAVA software. The quality control (QC) of raw reads was performed by removing reads containing adapter and ploy-N (N represents base information that cannot be determined)

and low quality reads to obtain clean reads. Meanwhile, Q20 (≥90%), Q30 (≥85%), and GC (40−50%) content of the clean reads were calculated for assessing the sequencing data and whether they meet the quality assurance (QA). Then, the clean reads were mapped to zebrafish genome reference sequence using HISAT2,[74] which can be used to exclude contamination from other species' genes. The read counts mapped to each gene were obtained using the featureCounts software,[75] and normalized to fragments per kilobase per million (FPKM) using the DEseq. 2 package.[76] The FPKM values of these expressed genes in each sample were used for principal component analysis (PCA) to assess between-group differences and within-group repeatability. DEG analysis was conducted using the DESeq. 2 package with $p_{adj} < 0.05$ and |log fold change|≥1. Based on the Kyoto Encyclopedia of Genes and Genomes (KEGG) database, DEGs were annotated to related signaling pathways for mechanistic studies. Finally, we performed protein−protein interaction (PPI) analysis for the DEGs in the related signaling pathway for the reference network in those pathway crosstalk analysis using STRING database (www.string-db.org) and Cytoscape software.

4.8. Statistical Analysis. Statistical analysis was performed using GraphPad Prism 7 software (GraphPad, La Jolla, CA). Experimental results were expressed as the mean ± standard deviation (SD) or as the mean ± the standard error of the mean (SEM). Statistical analyses were assessed using a one-way analysis of variance (ANOVA) with Dunnett's post-test. Differences were considered statistically significant at $p < 0.05$.

■ ASSOCIATED CONTENT

Ⓢ Supporting Information

The Supporting Information is available free of charge at https://pubs.acs.org/doi/10.1021/acsomega.2c06296.

> 1: Materials and methods; 2: Primer sequences (Tables S1 and S2); 3: KEGG pathways and DEGs of pathways (Tables S3−S7); 4: Mortality results, DEG counts, Schematic map of the cardiac contraction pathway, PPI analysis network diagram (Figures S1−S4); 5: Reference; DEG raw data (PDF)
>
> Glycosyl transferase (XLSX)

■ AUTHOR INFORMATION

Corresponding Authors

Chang Wang − *Hubei Key Laboratory of Environmental and Health Effects of Persistent Toxic Substances, School of Environment and Health, Jianghan University, Wuhan 430056, China; Division of Analytical and Environmental Toxicology, Department of Laboratory Medicine and Pathology, Faculty of Medicine and Dentistry, University of Alberta, Edmonton, Alberta T6G 2G3, Canada;* ⓘ orcid.org/0000-0002-2071-2799; Email: cwang@jhun.edu.cn

Xing-Fang Li − *Division of Analytical and Environmental Toxicology, Department of Laboratory Medicine and Pathology, Faculty of Medicine and Dentistry, University of Alberta, Edmonton, Alberta T6G 2G3, Canada;* ⓘ orcid.org/0000-0003-1844-7700; Email: xingfang.li@ualberta.ca

Authors

Xue Yang − *Hubei Key Laboratory of Environmental and Health Effects of Persistent Toxic Substances, School of Environment and Health, Jianghan University, Wuhan 430056, China*

Qi Zheng − *Hubei Key Laboratory of Environmental and Health Effects of Persistent Toxic Substances, School of Environment and Health, Jianghan University, Wuhan 430056, China;* ⓘ orcid.org/0000-0002-0138-0506

Qiongyu Liu − *Hubei Key Laboratory of Environmental and Health Effects of Persistent Toxic Substances, School of Environment and Health, Jianghan University, Wuhan 430056, China*

Nicholas J. P. Wawryk − *Division of Analytical and Environmental Toxicology, Department of Laboratory Medicine and Pathology, Faculty of Medicine and Dentistry, University of Alberta, Edmonton, Alberta T6G 2G3, Canada*

Complete contact information is available at:
https://pubs.acs.org/10.1021/acsomega.2c06296

Author Contributions

X.Y.: Methodology, investigation, data curation, formal analysis, validation, and writing − original draft. C.W.: Conceptualization and writing − review & editing. Q.Z.: Supervision, visualization, and funding acquisition. Q.L.: Data curation and investigation. N.J.P.W.: Writing − review & editing and investigation. X.-F.L. Project administration, writing − review & editing, and funding acquisition.

Notes

The authors declare no competing financial interest.

■ ACKNOWLEDGMENTS

■ REFERENCES

(1) Mitch, W. A.; Li, X.-F. Drinking water disinfection byproducts (DBPs) and human health effects: multidisciplinary challenges and opportunities. *Environ. Sci. Technol.* **2018**, *52*, 1681−1689.

(2) Richardson, S. D.; Ternes, T. A. Water analysis: emerging contaminants and current issues. *Anal. Chem.* **2022**, *94*, 382−416.

(3) Li, J. F.; Aziz, M. T.; Granger, C. O.; Richardson, S. D. Are disinfection byproducts (DBPs) formed in my cup of tea? Regulated, priority, and unknown DBPs. *Environ. Sci. Technol.* **2021**, *55*, 12994−13004.

(4) Liberatore, H. K.; Plewa, M. J.; Wagner, E. D.; VanBriesen, J. M.; Burnett, D. B.; Cizmas, L. H.; Richardson, S. D. Identification and comparative mammalian cell cytotoxicity of new iodo-phenolic disinfection byproducts in chloraminated oil and gas wastewaters. *Environ. Sci. Technol. Lett.* **2017**, *4*, 475−480.

(5) Liu, X. Y.; Chen, L.; Yang, M. T.; Tan, C. Q.; Chu, W. H. The occurrence, characteristics, transformation and control of aromatic disinfection by-products: A review. *Water Res.* **2020**, *184*, No. 116076.

(6) Yang, L.; Chen, X.; She, Q.; Cao, G.; Liu, Y.; Chang, V. W. C.; Tang, C. Y. Regulation, formation, exposure, and treatment of disinfection by-products (DBPs) in swimming pool waters: A critical review. *Environ. Int.* **2018**, *121*, 1039−1057.

(7) Cedergren, M. I.; Selbing, A. J.; Löfman, O.; Källen, B. A. Chlorination byproducts and nitrate in drinking water and risk for congenital cardiac defects. *Environ. Res.* **2002**, *89*, 124−130.

(8) Hwang, B. F.; Jaakkola, J. J.; Guo, H. R. Water disinfection by-products and the risk of specific birth defects: a population-based cross-sectional study in Taiwan. *Environ. Health* **2008**, *7*, 23.

(9) Wright, J. M.; Evans, A.; Kaufman, J. A.; Rivera-Núñez, Z.; Narotsky, M. G. Disinfection by-product exposures and the risk of specific cardiac birth defects. *Environ. Health Perspect.* **2017**, *125*, 269−277.

(10) Summerhayes, R. J.; Rahman, B.; Morgan, G. G.; Beresin, G.; Moreno, C.; Wright, J. M. Meta-analysis of small for gestational age births and disinfection byproduct exposures. *Environ. Res.* **2021**, *196*, No. 110280.

(11) Liu, C.; Wang, Y.; Chen, Y.; Sun, Y.; Huang, L.; Cheng, Y.; Liu, E.; Lu, W.; Messerlian, C. Blood and urinary biomarkers of prenatal exposure to disinfection byproducts and oxidative stress: A repeated measurement analysis. *Environ. Int.* **2020**, *137*, No. 105518.

(12) Rashid, C. S.; Bansal, A.; Simmons, R. A. Oxidative stress, intrauterine growth restriction, and developmental programming of type 2 diabetes. *Physiology* **2018**, *33*, 348−359.

(13) Biberoglu, E.; Biberoglu, K.; Kirbas, A.; Daglar, K.; Genc, M.; Avci, A.; Danisman, N. Circulating and myometrial markers of oxidative stress in pregnant women with fetal growth restriction. *J. Obstet. Gynaecol. Res.* **2016**, *42*, 29−35.

(14) Craven, C. B.; Blackstock, L. K. J.; Xie, J. J.; Li, J. H.; Yuan, C. G.; Li, X. F. Analytical discovery of water disinfection byproducts of toxicological relevance: highlighting halobenzoquinones. *Can. J. Chem.* **2021**, *99*, 715−724.

(15) Han, J.; Zhang, X.; Jiang, J.; Li, W. How much of the total organic halogen and developmental toxicity of chlorinated drinking water might be attributed to aromatic halogenated DBPs? *Environ. Sci. Technol.* **2021**, *55*, 5906−5916.

(16) Lou, J. X.; Lu, H. J.; Wang, W.; Zhu, L. Z. Molecular composition of halobenzoquinone precursors in natural organic matter in source water. *Water Res.* **2022**, *209*, No. 117901.

(17) Peng, F. Y.; Peng, J. J.; Li, H. P.; Li, Y.; Wang, B. Z.; Yang, Z. G. Health risks and predictive modeling of disinfection byproducts in swimming pools. *Environ. Int.* **2020**, *139*, No. 105726.

(18) Wagner, E. D.; Plewa, M. J. CHO cell cytotoxicity and genotoxicity analyses of disinfection by-products: An updated review. *J. Environ. Sci.* **2017**, *58*, 64−76.

(19) Yang, M. T.; Zhang, X. R. Comparative developmental toxicity of new aromatic halogenated dbps in a chlorinated saline sewage effluent to the marine polychaete *Platynereis dumerilii*. *Environ. Sci. Technol.* **2013**, *47*, 10868−10876.

(20) Jiang, J.; Zhang, X.; Zhu, X.; Li, Y. Removal of intermediate aromatic halogenated dbps by activated carbon adsorption: A new approach to controlling halogenated dbps in chlorinated drinking water. *Environ. Sci. Technol.* **2017**, *51*, 3435−3444.

(21) Liu, J.; Zhang, X. Comparative toxicity of new halophenolic DBPs in chlorinated saline wastewater effluents against a marine alga: Halophenolic DBPs are generally more toxic than haloaliphatic ones. *Water Res.* **2014**, *65*, 64−72.

(22) Kosaka, K.; Nakai, T.; Hishida, Y.; Asami, M.; Ohkubo, K.; Akiba, M. Formation of 2, 6-dichloro-1, 4-benzoquinone from aromatic compounds after chlorination. *Water Res.* **2017**, *110*, 48−55.

(23) Teo, T. L. L.; Coleman, H. M.; Khan, S. J. Chemical contaminants in swimming pools: Occurrence, implications and control. *Environ. Int.* **2015**, *76*, 16−31.

(24) Li, J. H.; Moe, B.; Vemula, S.; Wang, W.; Li, X. F. Emerging disinfection byproducts, halobenzoquinones: effects of isomeric structure and halogen substitution on cytotoxicity, formation of reactive oxygen species, and genotoxicity. *Environ. Sci. Technol.* **2016**, *50*, 6744−6752.

(25) Du, H. Y.; Li, J. H.; Moe, B.; McGuigan, C. F.; Shen, S. W.; Li, X. F. Cytotoxicity and oxidative damage induced by halobenzoquinones to T24 bladder cancer cells. *Environ. Sci. Technol.* **2013**, *47*, 2823−2830.

(26) Fu, K. Z.; Li, J. H.; Vemula, S.; Moe, B.; Li, X. F. Effects of halobenzoquinone and haloacetic acid water disinfection byproducts on human neural stem cells. *J. Environ. Sci.* **2017**, *58*, 239−249.

(27) Li, J. H.; Moe, B.; Liu, Y. M.; Li, X. F. Halobenzoquinone-induced alteration of gene expression associated with oxidative stress signaling pathways. *Environ. Sci. Technol.* **2018**, *52*, 6576−6584.

(28) Wang, W.; Qian, Y. C.; Li, J. H.; Aljuhani, N.; Siraki, A. G.; Le, X. C.; Li, X. F. Characterization of mechanisms of glutathione conjugation with halobenzoquinones in solution and HepG2 cells. *Environ. Sci. Technol.* **2018**, *52*, 2898−2908.

(29) Wang, C.; Yang, X.; Zheng, Q.; Moe, B.; Li, X. F. Halobenzoquinone-induced developmental toxicity, oxidative stress, and apoptosis in zebrafish embryos. *Environ. Sci. Technol.* **2018**, *52*, 10590−10598.

(30) Williams, R. Thanks be to zebrafish. *Circ. Res.* **2010**, *107*, 570−572.

(31) Poon, K. L.; Brand, T. The zebrafish model system in cardiovascular research: A tiny fish with mighty prospects. *Glob. Cardiol. Sci. Pract.* **2013**, *2013*, 9−28.

(32) Nikolova, G.; Lammert, E. Interdependent development of blood vessels and organs. *Cell Tissue Res.* **2003**, *314*, 33−42.

(33) Stainier, D. Y. R. Zebrafish genetics and vertebrate heart formation. *Nat. Rev. Genet.* **2001**, *2*, 39−48.

(34) Bakkers, J. Zebrafish as a model to study cardiac development and human cardiac disease. *Cardiovasc. Res.* **2011**, *91*, 279−288.

(35) Antkiewicz, D. S.; Burns, C. G.; Carney, S. A.; Peterson, R. E.; Heideman, W. Heart Malformation is an early response to TCDD in embryonic zebrafish. *Toxicol. Sci.* **2005**, *84*, 368−377.

(36) Sun, G.; Li, Y. Exposure to DBP induces the toxicity in early development and adverse effects on cardiac development in zebrafish (Danio rerio). *Chemosphere* **2019**, *218*, 76−82.

(37) Yang, X. X.; Liang, J. F.; Wu, Q.; Li, M.; Shan, W. Y.; Zeng, L.; Yao, L. L.; Liang, Y.; Wang, C.; Gao, J.; Guo, Y. Y.; Liu, Y.; Liu, R.; Luo, Q.; Zhou, Q. F.; Qu, G. B.; Jiang, G. B. Developmental toxicity of few-layered black phosphorus toward zebrafish. *Environ. Sci. Technol.* **2021**, *55*, 1134−1144.

(38) Ye, Q.; Liu, H. M.; Fang, C. X.; Liu, Y. S.; Liu, X. M.; Liu, J. R.; Zhang, C. Y.; Zhang, T. M.; Peng, C.; Guo, L. Cardiotoxicity evaluation and comparison of diterpene alkaloids on zebrafish. *Drug Chem. Toxicol.* **2021**, *44*, 294−301.

(39) Cunha, V.; Vogs, C.; Le Bihanic, F.; Dreij, K. Mixture effects of oxygenated PAHs and benzo[a]pyrene on cardiovascular development and function in zebrafish embryos. *Environ. Int.* **2020**, *143*, No. 105913.

(40) Xu, Z.; Ni, H.; Huang, Y.; Meng, Y.; Cao, Z.; Liao, X.; Zhang, S.; Guo, X.; Lu, H. Effect of fomesafen on the embryonic development of zebrafish. *Chemosphere* **2020**, *259*, No. 127380.

(41) Du, Z.; Hou, K.; Zhou, T.; Shi, B.; Zhang, C.; Zhu, L.; Li, B.; Wang, J.; Wang, J. Polyhalogenated carbazoles (PHCZs) induce cardiotoxicity and behavioral changes in zebrafish at early developmental stages. *Sci. Total Environ.* **2022**, *841*, No. 156738.

(42) Männer, J.; Wessel, A.; Yelbuz, T. M. How does the tubular embryonic heart work? Looking for the physical mechanism generating unidirectional blood flow in the valveless embryonic heart tube. *Dev. Dyn.* **2010**, *239*, 1035−1046.

(43) Isogai, S.; Horiguchi, M.; Weinstein, B. M. The vascular anatomy of the developing zebrafish: an atlas of embryonic and early larval development. *Dev. Biol.* **2001**, *230*, 278−301.

(44) Buschmann, I. R.; Lehmann, K.; Le-Noble, F. Physics meets molecules: is modulation of shear stress the link to vascular prevention. *Circ. Res.* **2008**, *102*, 510.

(45) Mi, P.; Tang, Y. Q.; Feng, X. Z. Acute fluorene-9-bisphenol exposure damages early development and induces cardiotoxicity in zebrafish (*Danio rerio*). *Ecotoxicol. Environ. Saf.* **2020**, *202*, No. 110922.

(46) Li, M.; Liu, X. Y.; Feng, X. Z. Cardiovascular toxicity and anxiety-like behavior induced by deltamethrin in zebrafish (*Danio rerio*) larvae. *Chemosphere* **2019**, *219*, 155−164.

(47) Rottbauer, W.; Wessels, G.; Dahme, T.; Just, S.; Trano, N.; Hassel, D.; Burns, C. G.; Katus, H. A.; Fishman, M. C. Cardiac myosin light chain-2. *Circ. Res.* **2006**, *99*, 323−331.

(48) Xin, Z. L.; Ma, Z. G.; Jiang, S.; Wang, D. J.; Fan, C. X.; Di, S. Y.; Hu, W.; Li, T.; She, J. J.; Yang, Y. FOXOs in the impaired heart: New therapeutic targets for cardiac diseases. *Biochim. Biophys. Acta, Mol. Basis Dis.* **2017**, *1863*, 486−498.

(49) Puigserver, P.; Rhee, J.; Donovan, J.; Walkey, C. J.; Yoon, J. C.; Oriente, F.; Kitamura, Y.; Altomonte, J.; Dong, H.; Accili, D.; Spiegelman, B. M. Insulin-regulated hepatic gluconeogenesis through FOXO1−PGC-1α interaction. *Nature* **2003**, *423*, 550−555.

(50) Ronnebaum, S. M.; Patterson, C. The FoxO family in cardiac function and dysfunction. *Annu. Rev. Physiol.* **2010**, *72*, 81−94.

(51) Sengupta, A.; Molkentin, J. D.; Yutzey, K. E. FoxO transcription factors promote autophagy in cardiomyocytes. *J. Biol. Chem.* **2009**, *284*, 28319−28331.

(52) Guo, Y. H.; Li, Z. P.; Shi, C. X.; Li, J.; Yao, M.; Chen, X. Trichostatin A attenuates oxidative stress-mediated myocardial injury through the FoxO3a signaling pathway. *Int. J. Mol. Med.* **2017**, *40*, 999−1008.

(53) Dumitrascu, G. R.; Bucur, O. Critical physiological and pathological functions of Forkhead Box O tumor suppressors. *Discoveries* **2013**, *1*, No. e5.

(54) Xing, W. J.; Zhang, X.; Li, J.; Dong, L.; Zhang, H. F.; Gao, F. Insulin and cardiovascular health-commemorating insulin centennial (in Chinese). *Sci. Sin. Vitae* **2021**, *51*, No. 351.

(55) Yu, Q. J.; Zhou, N.; Nan, Y.; Zhang, L. H.; Li, Y.; Hao, X. K.; Xiong, L. Z.; Lau, W. B.; Ma, X. L.; Wang, H. C.; Gao, F. Effective glycaemic control critically determines insulin cardioprotection against ischaemia/reperfusion injury in anaesthetized dogs. *Cardiovasc. Res.* **2014**, *103*, 238−247.

(56) Laustsen, P. G.; Russell, S. J.; Cui, L.; Entingh-Pearsall, A.; Holzenberger, M.; Liao, R.; Kahn, C. R. Essential role of insulin and insulin-like growth factor 1 receptor signaling in cardiac development and function. *Mol. Cell. Biol.* **2007**, *27*, 1649−1664.

(57) Yang, B. Y.; Zhai, G.; Gong, Y. L.; Su, J. Z.; Han, D.; Yin, Z.; Xie, S. Q. Depletion of insulin receptors leads to β-cell hyperplasia in zebrafish. *Sci. Bull.* **2017**, *62*, 486−492.

(58) Wilhelm, K.; Happel, K.; Eelen, G.; Schoors, S.; Oellerich, M. F.; Lim, R.; Zimmermann, B.; Aspalter, I. M.; Franco, C. A.; Boettger, T.; Braun, T.; Fruttiger, M.; Rajewsky, K.; Keller, C.; Brüning, J. C.; Gerhardt, H.; Carmeliet, P.; Potente, M. FOXO1 couples metabolic activity and growth state in the vascular endothelium. *Nature* **2016**, *529*, 216−220.

(59) He, L. C.; Lin, Y.; Day, D.; Teng, Y. B.; Wang, X. T.; Liu, X. L.; Yan, E.; Gong, J. C.; Qin, J.; Wang, X. L.; Xiang, J. B.; Mo, J. H.; Zhang, Y. P.; Zhang, J. F. J. Nitrated polycyclic aromatic hydrocarbons and arachidonic acid metabolisms relevant to cardiovascular pathophysiology: findings from a panel study in healthy adults. *Environ. Sci. Technol.* **2021**, *55*, 3867−3875.

(60) Lee, J. S.; Kang, H. M.; Jeong, C. B.; Han, J.; Park, H. G.; Lee, J. S. Protective role of freshwater and marine rotifer glutathione S-transferase sigma and omega isoforms transformed into heavy metal-exposed *Escherichia coli*. *Environ. Sci. Technol.* **2019**, *53*, 7840−7850.

(61) Liu, N.; Lin, F. J.; Chen, J.; Shao, Z. X.; Zhang, X. R.; Zhu, L. Z. Multistage defense system activated by tetrachlorobiphenyl and its hydroxylated and methoxylated derivatives in *Oryza sativa*. *Environ. Sci. Technol.* **2021**, *55*, 4889−4898.

(62) Doenst, T.; Nguyen, T. D.; Abel, E. D. Cardiac metabolism in heart failure implications beyond ATP production. *Circ. Res.* **2013**, *113*, 709−724.

(63) Schieber, M.; Chandel, N. S. Ros function in redox signaling and oxidative stress. *Curr. Biol.* **2014**, *24*, R453−R462.

(64) Zhu, B. Z.; Kalyanaraman, B.; Jiang, G. B. Molecular mechanism for metal-independent production of hydroxyl radicals by hydrogen peroxide and halogenated quinones. *Proc. Natl. Acad. Sci. U.S.A.* **2007**, *104*, 17575−17578.

(65) Zhu, B. Z.; Shan, G. Q.; Huang, C. H.; Kalyanaraman, B.; Mao, L.; Du, Y. G. Metal-independent decomposition of hydroperoxides by halogenated quinones: detection and identification of a quinone ketoxy radical. *Proc. Natl. Acad. Sci. U.S.A.* **2009**, *106*, 11466−11471.

(66) Agalakova, N. I.; Gusev, G. P. Fluoride induces oxidative stress and ATP depletion in the rat erythrocytes in vitro. *Environ. Toxicol. Pharmacol.* **2012**, *34*, 334−337.

(67) Hemalatha, K. L.; Prince, P. S. M. Preventive effects of zingerone on cardiac mitochondrial oxidative stress, calcium ion overload and adenosine triphosphate depletion in isoproterenol induced myocardial infarcted rats. *RSC Adv.* **2016**, *6*, 112332−112339.

(68) Goth, L.; Eaton, J. W. Hereditary catalase deficiencies and increased risk of diabetes. *Lancet* **2000**, *356*, 1820−1821.

(69) Krysko, O.; Hulshagen, L.; Janssen, A.; Schuetz, G.; Klein, R.; De Bruycker, M.; Espeel, M.; Gressens, P.; Baes, M. Neocortical and cerebellar developmental abnormalities in conditions of selective elimination of peroxisomes from brain or from liver. *J. Neurosci. Res.* **2007**, *85*, 58−72.

(70) Schrader, M.; Fahimi, H. D. Peroxisomes and oxidative stress. *Biochim. Biophys. Acta, Mol. Cell Res.* **2006**, *1763*, 1755−1766.

(71) Wallner, S.; Schmitz, G. Plasmalogens the neglected regulatory and scavenging lipid species. *Chem. Phys. Lipids* **2011**, *164*, 573−589.

(72) Weiss, R. G.; Gerstenblith, G.; Bottomley, P. A. ATP flux through creatine kinase in the normal, stressed, and failing human heart. *Proc. Natl. Acad. Sci. U.S.A.* **2005**, *102*, 808−813.

(73) Wu, Y.; Wei, W. Z.; Luo, J.; Pan, Y.; Yang, M. T.; Hua, M.; Chu, W. H.; Shuang, C. D.; Li, A. M. Comparative toxicity analyses from different endpoints: are new cyclic disinfection byproducts (DBPs) more toxic than common aliphatic DBPs? *Environ. Sci. Technol.* **2022**, *56*, 194−207.

(74) Kim, D.; Langmead, B.; Salzberg, S. L. HISAT: a fast spliced aligner with low memory requirements. *Nat. Methods* **2015**, *12*, 357−360.

(75) Liao, Y.; Smyth, G. K.; Shi, W. featureCounts: an efficient general purpose program for assigning sequence reads to genomic features. *Bioinformatics* **2014**, *30*, 923−930.

(76) Love, M. I.; Huber, W.; Anders, S. Moderated estimation of fold change and dispersion for RNA-seq data with DESeq. 2. *Genome Biol* **2014**, *15*, 1−21.